IIE Transactions

ISSN: 0740-817X (Print) 1545-8830 (Online) Journal homepage: http://www.tandfonline.com/loi/uiie20

Multiscale monitoring of autocorrelated processes using wavelets analysis

Huairui Guo , Kamran Paynabar & Jionghua Jin

To cite this article: Huairui Guo , Kamran Paynabar & Jionghua Jin (2012) Multiscale monitoring of autocorrelated processes using wavelets analysis, IIE Transactions, 44:4, 312-326, DOI: 10.1080/0740817X.2011.609872

To link to this article: http://dx.doi.org/10.1080/0740817X.2011.609872

Accepted author version posted online: 08 Aug 2011.

IIE Transactions (2012) **44**, 312–326

ISSN: 0740-817X print / 1545-8830 online
DOI: 10.1080/0740817X.2011.609872

Multiscale monitoring of autocorrelated processes using wavelets analysis

HUAIRUI GUO[1], KAMRAN PAYNABAR[2] and JIONGHUA JIN[2,*]

[1] *ReliaSoft Corporation, 1450 South Eastside Loop, Tucson, AZ 85710, USA*
[2] *Department of Industrial and Operations Engineering, The University of Michigan, Ann Arbor, MI 48109, USA*
E-mail: jhjin@umich.edu

Received October 2009 and accepted January 2011

This article proposes a new method to develop multiscale monitoring control charts for an autocorrelated process that has an underlying unknown ARMA(2, 1) model structure. The Haar wavelet transform is used to obtain effective monitoring statistics by considering the process dynamic characteristics in both the time and frequency domains. Three control charts are developed on three selected levels of Haar wavelet coefficients in order to simultaneously detect the changes in the process mean, process variance, and measurement error variance, respectively. A systematic method for automatically determining the optimal monitoring level of Haar wavelet decomposition is proposed that does not require the estimation of an ARMA model. It is shown that the proposed wavelet-based Cumulative SUM (CUSUM) chart on Haar wavelet detail coefficients is only sensitive to the variance changes and robust to process mean shifts. This property provides the separate monitoring capability between a variance change and a mean shift, which shows its advantage by comparison with the traditional CUSUM monitoring chart. For the purpose of mean shift detection, it is also shown that using the proposed wavelet-based Exponentially Weighted Moving Average (EWMA) chart to monitor Haar wavelet scale coefficients will more successfully detect small mean shifts than direct-EWMA charts.

Keywords: ARMA model, autocorrelated process, multiscale control charts, wavelet analysis, Haar decomposition

1. Introduction

The increasing amount of automation used in manufacturing processes has resulted in the obtained sensor data used in process control functions being increasingly autocorrelated. It is known that a process fault may occur at an unknown time as a result of either a single mean or a single variance change or both. In general, the root causes that lead to a mean shift or variance change may be different. Therefore, it is always desirable to develop effective process monitoring charts that can not only detect process changes but also differentiate between faults caused by a mean shift or a variance change. In this article multiscale process monitoring charts based on Haar wavelets analysis are investigated for this purpose.

To monitor autocorrelated data, one of the popularly used model-based methods is a Special Cause Chart (SCC; Alwan and Roberts, 1988; Wardell *et al.*, 1992). The principle of the SCC method is to whiten an autocorrelated process based on the process model and then use conventional control charts to monitor the whitened residuals. The performance of an SCC chart, however, is very sensitive to the model's estimation accuracy (Apley and Shi, 1999). Dyer *et al.* (2003) proposed a reverse moving average control chart based on residuals as a new model-based monitoring technique, compared it with traditional methods, and made recommendations for the most appropriate chart to use for a variety of AR(1), MA(1), and ARMA(1, 1) processes.

To avoid the effort required for time series modeling studies, a batch means control chart (Runger and Willemain, 1996) was developed by organizing the observations into adjacent non-overlapping batches of equal size to ensure that the batch means were approximately identically independently distributed (i.i.d.), and then the traditional Statistical Process Control (SPC) charts were applied. However, only the AR(1) process was considered in the analysis. For detecting a small process mean shift, the EWMAST chart or Direct Exponentially Weighted Moving Average (Direct-EWMA) chart (Schmid, 1997; Adams and Tseng, 1998; Zhang, 1998; Lu and Reynolds, 1999) was developed by directly applying the EWMA statistics to autocorrelated data without having to estimate the underlying process model. It was shown that Direct-EWMA charts are very effective at detecting a small mean shift in a slowly varying process.

To detect a small variance change using individual observations, the Standard Deviation Cumulative SUM

*Corresponding author

(SD-CUSUM) chart was developed by Hawkins (1981, 1993). However, this chart cannot distinguish between a mean shift and a variance change. Moreover, it will be shown later in this article that the performance of these control charts is dramatically degraded for an autocorrelated process of ARMA(n, m) ($n \geq 2$). Considering the uncertainty in the estimates of the in-control true mean and variance, Hawkins and Zamba (2005) proposed a combined single chart to detect a mean shift, a variance change, or both based on the unknown-parameter change-point model. To effectively detect both small and large mean shifts, Capizzi and Masarotto (2003) suggested an Adaptive EWMA (AEWMA) chart to include both EWMA and Shewhart charts. In fact, the EWMA model is a special case of the ARMA (1, 1) model with the underlying IMA(1, 1) model structure. When a process has an underlying ARMA (2, 1) model with stochastic periodic characteristics, which is presented by a pair of complex characteristic roots in the characteristic equation of an ARMA(n, m) model, the effectiveness of an EWMA chart will be significantly affected. This will be shown later in this article.

To simultaneously detect mean shifts and variance changes, Reynolds and Stoumbos (2006) developed AEWMA-type charts based on squared deviations from a target value that numerically compares the results with the combination of control charts for the simultaneous monitoring of mean shifts and variance changes; no autocorrelation cases were considered, however. Very little research has been done in the area of simultaneously monitoring both mean shifts and variance changes for autocorrelated data, except for the work by Hwarng (2005), who proposed a neural network–based identification system to detect both mean shifts and correlation parameter changes for AR(1) processes. Therefore, it is necessary to develop new control charts for autocorrelated processes that have strong dynamic characteristics with an unknown high-order ARMA(n, m) ($n \geq 2$) model representation.

Recently, wavelet-based SPC methods have been increasingly used in various research efforts (Bakshi, 1998, 1999; Luo *et al.*, 1999; Jin and Shi, 2001; Lada *et al.*, 2002; Ganesan *et al.*, 2003; Jeong *et al.*, 2006; Chicken *et al.*, 2009). All of those monitoring methods, however, were specifically developed for the purpose of monitoring multivariate mean shifts without considering process variance changes. In the research discussed in this article, unlike existing research, the proposed multiscale control charts are developed based on original time series measurement data, allowing the monitoring of both process mean and variance changes for a process with an underlying ARMA(n, m) ($n = 2$) model. A new method is proposed that automatically selects the optimal monitoring levels of Haar wavelets coefficients that not only reduces the overall false alarm rate but also simplifies the root cause diagnosis through the identification of process fault types due to either a mean shift, a variance change, or both.

It will also be shown that the determination of the optimal monitoring levels is based on the fundamental principle of the process dynamic characteristics in both time and frequency domains. Although the autospectrum analysis of an ARMA model is used as the theoretical basis to determine the optimal monitoring levels in the analysis, the implementation of choosing an optimal monitoring level does not require identifying and estimating an ARMA model from data. In this sense, the proposed method of multiscale monitoring charts has the merit of being a model-free approach.

The rest of this article is organized as follows: Section 2 is used to define the research scope, in which the investigated process together with the interested process faults are described, and the design and performance of the related control charts are briefly reviewed. Section 3 gives a framework overview of the proposed multiscale monitoring system, and Section 4 discusses details of the proposed methodology, with Section 4.1 discussing the variance change detection for both process variance and measurement error variance. Two corresponding wavelet-based SD-CUSUM charts are developed in this subsection, and a systematic method for selecting the optimal monitoring levels of detail coefficients is addressed. Regarding detection of a small mean shift, Section 4.2 investigates how to develop a wavelet-based EWMA chart on the selected level of scale coefficients. Several case studies are given in Section 5. Finally, the article concludes in Section 6.

2. Description of process fault characteristics and review of related control charts

2.1. *Description of process faults*

An autocorrelated stationary process under a normal operation condition can be generally described by an ARMA(n, m) model as (Box *et al.*, 1994):

$$A(q)x_t = D(q)a_t, \tag{1}$$

where the process noise a_t is an i.i.d. Gaussian process with $a_t \sim NID(0, \sigma_a^2)$, and x_t is the process actual output. $A(q)$ and $D(q)$ are polynomial functions of the backshift operator denoted as $q^{-1}(q^{-1}x_t = x_{t-1})$, which are defined as AR and MA as follows, respectively:

$$A(q) = 1 - \phi_1 q^{-1} - \phi_2 q^{-2} - \cdots - \phi_n q^{-n}, \tag{2}$$
$$D(q) = 1 - \theta_1 q^{-1} - \theta_2 q^{-2} - \cdots \theta_m q^{-m}. \tag{3}$$

We also consider the inevitable measurement errors of $e_t \sim NID(0, \sigma_e^2)$, which is assumed to be independent of process noise a_t as shown in Fig. 1. Thus, the autocorrelated measurement data y_t, which are under a normal operation

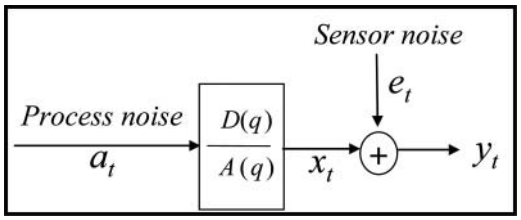

Fig. 1. Process model structure.

condition, are generally modeled by

$$y_t = x_t + e_t,$$
$$x_t = \phi_1 x_{t-1} + \cdots \phi_n x_{t-n} - \theta_1 a_{t-1} - \cdots - \theta_m a_{t-m} + a_t. \tag{4}$$

Therefore, under the normal process condition, we have $H_0 : y_t \sim N(0, \sigma_x^2 + \sigma_e^2)$. Since σ_x^2 is a linear function of σ_a^2 (to be shown in Equation (16)) and the process model parameters $D(q)/A(q)$ are not changed, the root cause of the process variance change on σ_x^2 is assumed to be due to the change of σ_a^2. Therefore, σ_a^2 is monitored to reflect the change of the process variance. In this article, process monitoring control charts will be developed to detect the occurrence of the following possible process faults:

$$\begin{aligned}
&\text{Fault 1 (process variance change):} && H_1^1 : a_t \sim N\left(0, \delta_a^2 \sigma_a^2\right),\\
&\text{Fault 2 (measurement errors variance change):} && H_1^2 : e_t \sim N\left(0, \delta_e^2 \sigma_e^2\right),\\
&\text{Fault 3 (process mean shift):} && H_1^3 : a_t \sim N\left(\mu_a, \sigma_a^2\right),
\end{aligned} \tag{5}$$

where Fault 1 and Fault 2 correspond to the variance change with the change ratio of $\delta_a > 1$ and $\delta_e > 1$, respectively, and Fault 3 corresponds to the mean shift with the relative shift of $\delta_\mu = \mu_a/\sigma_a$. All three faults are sustained in process changes, in which only an increase in variance is considered. The procedures for monitoring those faults will be discussed in Section 4.

Unlike existing research, which mainly focuses on autocorrelated processes with a slow dynamic change behavior described by an AR(1) or ARMA(1, 1) model, this research will focus more on a higher-order autocorrelated processes represented by ARMA(2, 1), which has a pair of complex roots in the characteristic equation of the ARMA(2, 1) model (Pandit and Wu, 1993). To have a general representation in this article, the normalized frequency is used; it is calculated as the ratio of the actual system frequency f to the sampling frequency f_{sampling}. If f_c is used to denote the actual system characteristic frequency, then $0.05 < f_c/f_{\text{sampling}} < 0.5$ is held in the article, where the upper bound $2f_c < f_{\text{sampling}}$ is constrained to meet the requirement of the Shannon sampling theorem (Pandit and Wu, 1983), and the lower bound $f_c > 0.05\ f_{\text{sampling}}$ is set to consider the minimal frequency of a dynamic system's behavior (at least 10% of the upper bound). As examples, three ARMA(2, 1) models representing different dynamics (given in Table 1) will be used for the following analyses in this article. All models are stable since all their characteristic roots are in the unit circle (Pandit and Wu, 1983).

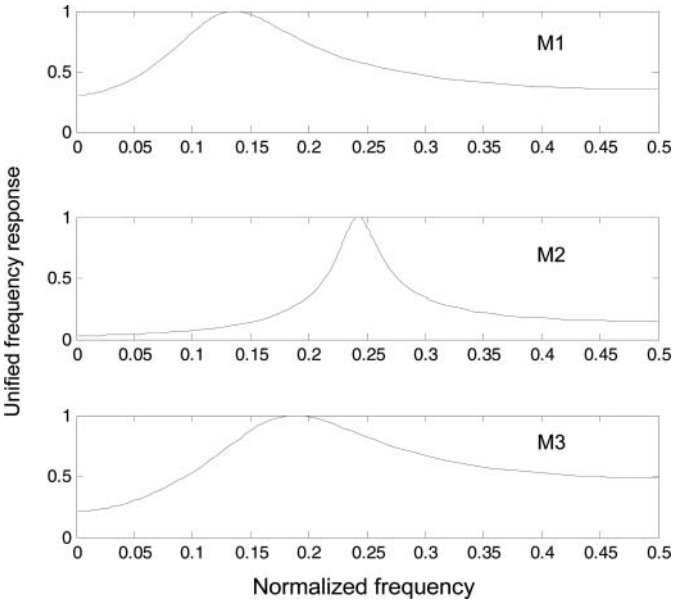

Fig. 2. Autospectrums of the models listed in Table 1.

The theoretical autospectra representation of x_t under the normal process condition in Equation (1) can be obtained as (Pandit and Wu, 1983):

$$f_0^x(\omega) = \frac{\Delta_t \sigma_a^2}{2\pi} \frac{|e^{mi\omega\Delta_t} - \theta_1 e^{(m-1)i\omega\Delta_t} - \cdots - \theta_m|^2}{|e^{ni\omega\Delta_t} - \phi_1 e^{(n-1)i\omega\Delta_t} - \cdots - \phi_n|^2}, \tag{6}$$

where $\omega = 2\pi f$ is the angular frequency in radians per unit time, and $\Delta_t = 1/f_{\text{sampling}}$ is the sampling interval. Figure 2

Table 1. Exemple models and their characteristics

Model	*Parameters*		*Characteristic roots*	*Normalized characteristic frequency* f_c/f_{sampling}
	$A(q)$	$D(q)$		
Model 1 (M1)	$1 - 0.99q^{-1} + 0.49q^{-2}$	$1 - 0.7q^{-1}$	$0.4950 \pm 0.4949i$	0.125
Model 2 (M2)	$1 - 0.1q^{-1} + 0.8q^{-2}$	$1 - 0.7q^{-1}$	$0.0500 \pm 0.8930i$	0.241
Model 3 (M3)	$1 - 0.6q^{-1} + 0.4q^{-2}$	$1 - 0.7q^{-1}$	$0.3000 \pm 0.5568i$	0.171

shows the autospectra of the three models listed in Table 1, which clearly reflects their different dynamic characteristics. In the figure, the y-axis represents the unified system frequency response, which is calculated as the ratio of the actual system frequency response in Equation (6) to the maximum system frequency response. The x-axis represents the normalized frequency relative to the sampling frequency.

2.2. *Review of related control charts*

2.2.1. *Review of SD-CUSUM charts for variance change detection and their limitations*

For monitoring the process variance, a standard SD-CUSUM chart assumes that each observation y_i is normally distributed with $y_i \sim N(\mu_0, \sigma^2)$. The standardized monitoring statistic v_i is defined as (Hawkins, 1981):

$$z_i = \frac{|y_i - \mu_0|}{\sigma}. \tag{7}$$

$$v_i = \frac{(\sqrt{z_i} - 0.822)}{0.349}. \tag{8}$$

Two one-sided standardized standard deviation CUSUM S_i^+ and S_i^- can be established as follows:

$$\begin{aligned} S_i^+ &= \max[0, v_i - K + S_{i-1}^+], \\ S_i^- &= \max[0, -K - v_i + S_{i-1}^-], \end{aligned} \tag{9}$$

where $S_0^+ = S_0^- = 0$, and the values of K and h are selected based on the regular CUSUM chart, denoted as M-CUSUM, for monitoring a process mean shift.

Although the monitoring statistic v_i is specifically designed for monitoring the variance change, it may actually generate alarm signals under mean shifts, even if there are no variance changes. Hawkins (1993) suggested plotting two CUSUM charts for the mean and standard deviation monitoring together. If only the SD-CUSUM shows the system being in an out-of-control state, one would suspect a change in variance; but if both the SD-CUSUM and M-CUSUM charts signal the system being in an out-of-control state, one would suspect a shift in the mean. When a process has both a standard deviation change and a mean shift, however, it may cause the misdetection of a mean shift, as shown in Fig. 3.

In Fig. 3, Model 1 in Table 1 is used with the distribution of a_t changing from $N(0, 1)$ to $N(1, 2.5^2)$ from time $\tau = 51$. Because of the variance change, the M-CUSUM chart for the mean shift detection shows a fluctuation pattern instead of an increasing drift pattern. Therefore, those two CUSUM charts are not sufficient to identify whether the process change is due to a mean shift, a standard deviation change, or both.

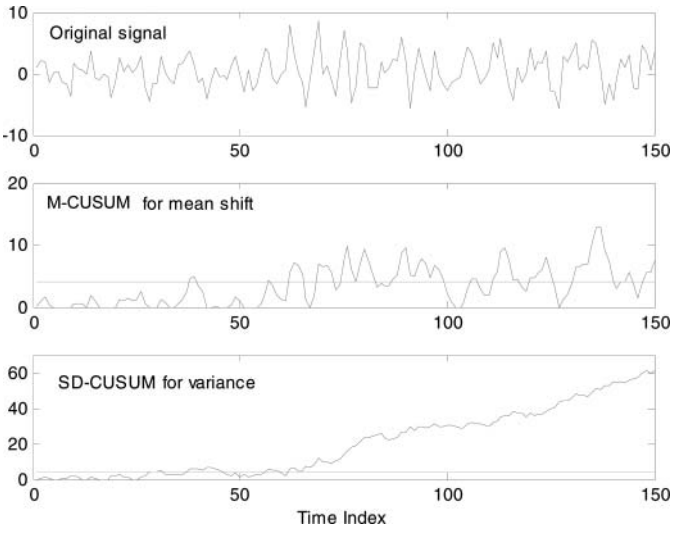

Fig. 3. Misdetection of a mean shift using a CUSUM chart under a variance change.

2.2.2. *Review of EWMA charts for mean shift detection and their limitations*

The EWMA chart is widely used to detect a small mean shift (Montgomery, 2005). In this article, the control limits of EWMA charts will be set up to make the in-control Average Run Length (ARL_0) approximately equal to 370 with $\lambda = 0.2$ (Montgomery, 2005). The following simulation results illustrate some limitation of applying the existing EWMA directly to observations (i.e., Direct-EWMA) and to residuals (i.e., SCC-EWMA) when both mean and variance changes occur in an autocorrelated process. In this simulation, Model 1 is used and the distribution of a_t changes from $N(0, 1)$ to $N(1, 2^2)$ from time $\tau = 51$. The SCC-EWMA is applied to the model residuals based on the estimated model parameters when the true model structure is given, whereas the Direct-EWMA is applied directly to the original signal. The control limits are ± 0.9583 and ± 0.9983, corresponding to SCC-EWMA and Direct-EWMA, respectively.

As shown in the control charts of Fig. 4, the detection performance of the Direct-EWMA as a model-free approach is severely affected by the process variance change. Moreover, for the SCC-EWMA, even though the true model structure is used and the estimated parameters are close to the true parameters, the detection performance of a mean shift also fluctuates due to the additional variance change. Therefore, it is necessary to develop a new approach for detecting a mean shift in the presence of a variance change for an autocorrelated process with a high characteristic frequency.

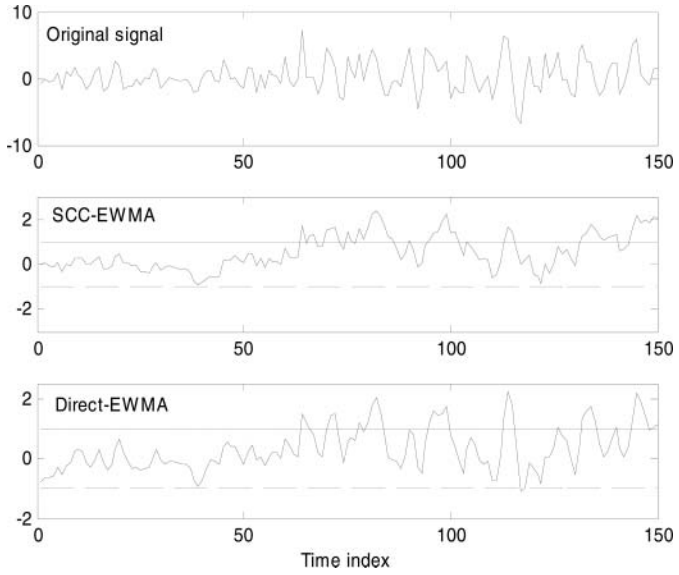

Fig. 4. Effect of a variance change on EWMA charts for mean shift detection.

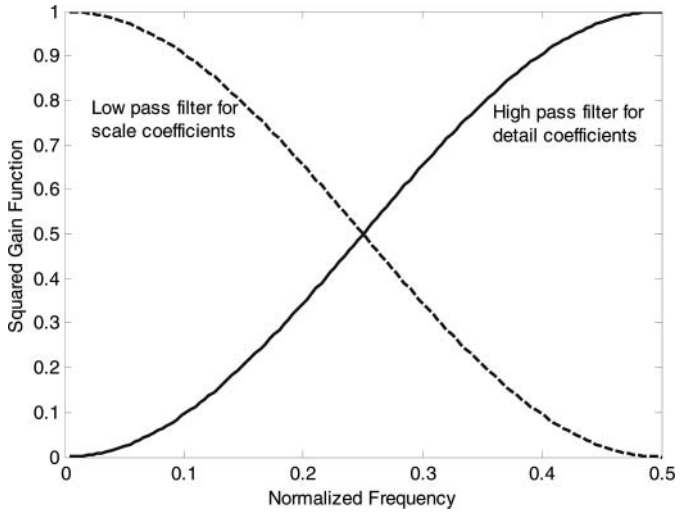

Fig. 6. Filter frequency response using the Haar transform.

3. Proposed framework of a multiscale monitoring system

3.1. *Multiscale monitoring through wavelet decomposition using the Haar transform*

If $y(t)$ is an integrable function on $L^2(R)$, i.e., $\int_{-\infty}^{+\infty} y(t)^2 \mathrm{d}t < \infty$, it can be fully expressed by wavelets decomposition (Daubechies, 1992). The widely used Haar transform is the first-order Daubechies wavelet transform, denoted as DB1. For an incoming signal y_t, the Haar transform of y_t can be easily obtained by using filter banks. As shown in Fig. 5, h_j and l_j are the corresponding high-pass and low-pass filters at the decomposition level j, which are defined as

$$h_j = \frac{1}{\sqrt{2}}[1 \; -1], \quad l_j = \frac{1}{\sqrt{2}}[1 \;\; 1] \quad j = 1, 2, \ldots \tag{10}$$

The unified frequency responses of filters h_j and l_j are given in Fig. 6. Based on the above wavelet filter bank using the Haar basis, the scale coefficients $c^y_{j,k}$ and detail coefficients $d^y_{j,k}$ can be obtained by

$$c^y_{j,k} = \frac{[(y_k + \cdots + y_{k-2^j+1})]}{2^{j/2}}. \tag{11}$$

$$d^y_{j,k} = [(y_{k-2^j+1} + \cdots + y_{k-2^{j-1}}) - (y_{k-2^{j-1}+1} + \cdots + y_k)]/2^{j/2}. \tag{12}$$

Based on the frequency responses of the Haar transform as shown in Fig. 6, it can be seen that the high-pass filter used to generate the detail coefficients $d^y_{j,k}$ will suppress the low-frequency components, whereas the low-pass filter used to obtain the scale coefficients $c^y_{j,k}$ will suppress the high-frequency components. Later sections will discuss the point that the detail coefficients obtained from high-pass filters at different levels mainly reflect the signal variance change (Section 4.1), whereas the scale coefficients obtained from the low-pass filter mainly reflect the signal mean shift (Section 4.2). Moreover, different decomposition levels of detail coefficients lead to different detection powers for process variance change (Fault 1) and the measurement error variance change (Fault 2); these will be discussed in Sections 4.1.2 and 4.1.3, respectively.

The proposed multiscale monitoring system consists of three monitoring charts as shown in Fig. 7; these are used

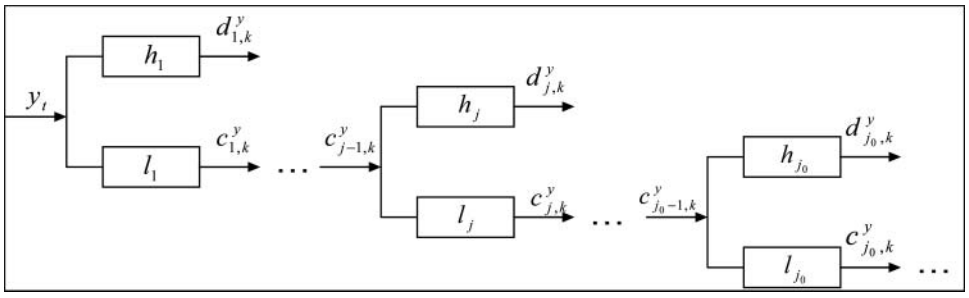

Fig. 5. Filter bank structure for the Haar wavelet transform.

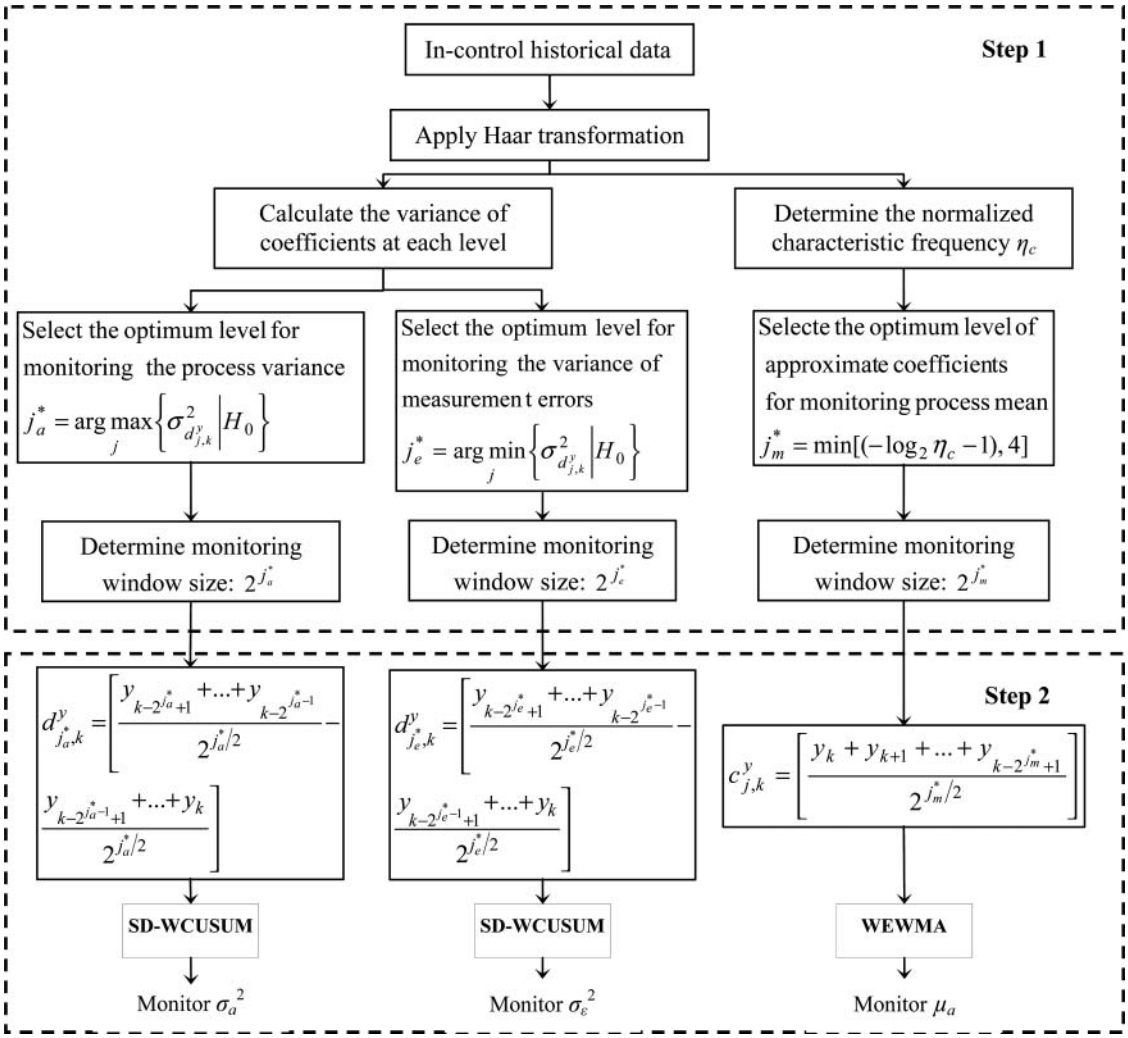

Fig. 7. Two steps for constructing the proposed multiscale monitoring system.

to monitor the changes of process variance (σ_a^2), measurement error variance (σ_e^2), and process mean (μ_a). There are two steps in constructing these three control charts. In Step 1, the optimal decomposition levels of the monitored Haar wavelet coefficients are determined for each control chart based on historical in-control data. In Step 2, the monitoring statistics and the associated control limits are constructed for the three monitoring charts based on the corresponding optimal monitoring levels j^* selected at Step 1. Without loss of generality, it is assumed that during online process monitoring, the process is in an in-control state up to time k, with $k \geq 2^{j*}$ (j^* is the selected optimal level). The wavelet coefficients, which are calculated using Equations (11) and (12), are used as monitoring statistics for detecting future process changes. Therefore, these scale coefficients (Equation (11)) and detail coefficients (Equation (12)) under the Haar transform can also be equivalently considered as the average and the range statistics within the selected monitoring window, the size of which is determined by the selected optimal decomposition level at Step 1. A detailed description of how to select the optimal monitoring level and how to use each of three monitoring charts will be presented in the following subsection.

3.2. *Multiscale monitoring scheme for detecting both mean and variance changes*

As shown in Fig. 7, three monitoring charts are simultaneously used as an integrated monitoring system to detect whether one or multiple process faults occur for given samples. If any control chart signals an out-of-control situation, it indicates that the corresponding fault may possibly occur. A summary of the monitoring scheme and procedures for the monitoring chart design are now presented. The details for optimal selection of the monitoring level of the Haar coefficients will be discussed in Section 4.

1. A wavelet-based SD-CUSUM (SD-WCUSUM) chart for detecting a process variance change (Fault 1). This chart (Step 2 of Fig. 7) is used to detect a process

variance change by monitoring the selected level of the detail coefficients ($\delta_a > 1$). The optimal level is selected so that the monitored detail coefficients, which are calculated at each level of Haar wavelet decompositions based on the in-control condition data, have the maximum variance among all decomposition levels (The detailed proof will be presented in Section 4.1.2.) After selecting an optimal level (in Step 2 of Fig. 7), the design and use of the SD-WCUSUM chart based on the selected detail coefficients are similar to those of a regular SD-CUSUM chart.

2. An SD-WCUSUM chart for detecting a variance change of measurement errors (Fault 2). Similar to the detection of a process variance change, another SD-WCUSUM (Step 2 of Fig. 7) is developed to detect a variance change in measurement errors ($\delta_e > 1$) but at a different level of the detail coefficients. The optimal monitoring level is selected so that the monitored detail coefficients, which are calculated at each level of Haar wavelet decompositions based on the in-control condition data, have the minimum variance among all decomposition levels. (The detailed proof will be presented in Section 4.1.3.) After selecting an optimal level (in Step 2 of Fig. 7), the design and usage of the SD-WCUSUM chart based on the selected detail coefficients are similar to those of a regular SD-CUSUM chart.
3. A wavelet-based EWMA (WEWMA) chart for detecting a process mean shift (Fault 3). This chart (Step 2 of Fig. 7) is developed to monitor the scale coefficients for process mean shift detection ($\delta_u \neq 0$); this is different from the variance monitoring using the detail coefficients. The selection of an optimal decomposition level (Stage 1 in Fig. 7) will be determined based on the dynamic characteristics of autocorrelated data, which will be discussed in Section 4.2.

4. Multiscale monitoring chart development

The proposed multiscale monitoring system is developed to have the following merits.

1. It can simultaneously monitor multiple process faults.
2. Monitoring of the mean shift and variance change is conducted at different frequency ranges through scale coefficients via a low-pass filter and through detail coefficients via a high-pass filter at different levels. This leads to a better separability or robustness for identifying a process change between a mean shift and a variance change or both changes.
3. When any of these monitoring charts show an out-of-control situation, it not only signals a possible process fault but also indicates what type of process change; this differentiation can help expedite the fault diagnosis and decision making for process correction.

The details of the methodology development will be shown in the following subsections.

4.1. *SD-WCUSUM chart for variance change detection*

4.1.1. *Relationship between detail coefficient variance and process variance*

Since Haar wavelet coefficients are used as the monitoring features, this subsection will present a remark that explains the relationship between the variance of detail coefficients and process variance.

Remark 1. The variance of the Haar detail coefficients is proportional to the process variance plus an additive measurement error variance; i.e., $\sigma^2_{d^y_{j,k}} = \rho_j \sigma_a^2 + \sigma_e^2$, where the proportional constant ρ_j is solely determined by the wavelet decomposition level j for a given ARMA model.

Justification: Based on the impulse response representation of the model in Equation (1), the system's actual output under normal conditions can be obtained as

$$x_t = \sum_{k=0}^{\infty} g_k a_{t-k},$$

where g_k is the impulse response function or Green's function (Pandit and Wu, 1983). It is known that if a process is stable, g_k will converge to zero when k is large enough (e.g., $k > M$). Thus, x_t can be further written as

$$x_t = \sum_{k=0}^{M} g_k a_{t-k}. \tag{13}$$

The covariance of x_t and x_{t-s} can be obtained as (Pandit and Wu, 1983):

$$\operatorname{cov}(x_t, x_s) = \sigma_a^2 \sum_{k=s}^{M} g_{k-s} g_k = r_s \sigma_a^2, \tag{14}$$

where $r_s = \sum_{k=s}^{M} g_{k-s} g_k$. Since $y_t = x_t + e_t$, the covariance of y_t and y_{t-s} is obtained as follows:

$$\operatorname{cov}(y_t, y_{t-s}) = \begin{cases} \sigma^2_{x_t} + \sigma_e^2 = \sigma_e^2 + r_0 \sigma_a^2, & s = 0, \\ \operatorname{cov}(x_t, x_{t-s}) = r_s \sigma_a^2, & s \neq 0. \end{cases} \tag{15}$$

Hence, the variance of the Haar detail coefficient $d^y_{j,k}$ is

$$\begin{aligned} \sigma^2_{d^y_{j,k}} &= \operatorname{var}\{[(y_{k-2^j+1} + \cdots + y_{k-2^{j-1}}) \\ &\quad - (y_{k-2^{j-1}+1} + \cdots + y_k)]/2^{j/2}\} \\ &= \sigma_e^2 + \sigma_a^2 \left\{ r_0 + r_{2^{j-1}} + (1/2^j) \left[\sum_{i=1}^{2^{j-1}-1} (2^{j+1} - 6i) r_i \right.\right. \\ &\quad \left.\left. - 2 \sum_{i=1}^{2^{j-1}-1} (i \times r_{n-i}) \right] \right\} \\ &= \sigma_e^2 + \sigma_a^2 \rho_j, \end{aligned} \tag{16}$$

where ρ_j represents all the terms in the bracket, which is a constant coefficient at a given decomposition level j for a given time-invariant system.

The conclusion here is that the variance of Haar detail coefficients is proportional to the variance σ_a^2 plus an additional σ_e^2. Moreover, the different levels of j have a different sensitivity ρ_j to process variance σ_a^2. Therefore, such an optimal monitoring level can be found to have the most sensitive detail coefficients to the variance change. The details will be discussed in the following subsection.

4.1.2. *Select the optimal level of Haar detail coefficients for detecting a process variance change*

This subsection presents Rule 1, which explains how the optimal level is selected for monitoring a process variance change.

Rule 1: The optimal level of Haar detail coefficients for monitoring a process variance change is selected so that the chosen level has the maximum variance of detail coefficients among all decomposition levels of in-control data; that is,

$$j_a^* = \arg\max_j \left\{ \sigma^2_{d^y_{j,k}} \,\middle|\, H_0 \right\}.$$

Justification: Based on Section 2, it is known that the distributions of process noise a_t under the in-control condition (H_0) and under the process variance change condition (H_1^1) are

$$\begin{aligned} \mathrm{H}_0 &: a_t \sim N\left(0, \sigma_a^2\right), \\ H_1^1 &: a_t \sim N\left(0, \delta_a^2 \sigma_a^2\right). \end{aligned} \tag{17}$$

It follows from Remark 1 that the distributions of the Haar detail coefficients under H_0 and H_1^1 (Fault 1) are

$$\begin{aligned} H_0 &: d^y_{j,k} \sim N\left(0, \rho_j \sigma_a^2 + \sigma_e^2\right), \\ H_1^1 &: d^y_{j,k} \sim N\left(0, \delta_a^2 \rho_j \sigma_a^2 + \sigma_e^2\right). \end{aligned} \tag{18}$$

Therefore, the variance change ratio $\delta^a_{d_j}$ of the Haar detail coefficients under H_0 and H_1^1 (Fault 1) can be obtained as

$$\begin{aligned} \delta^a_{d_j} &= \frac{\sigma^2_{d^y_{j,k}|H_1^1}}{\sigma^2_{d^y_{j,k}|H_0}} = \frac{\delta_a^2 \rho_j \sigma_a^2 + \sigma_e^2}{\rho_j \sigma_a^2 + \sigma_e^2} = \frac{\delta_a^2 \rho_j \sigma_a^2/\sigma_e^2 + 1}{\rho_j \sigma_a^2/\sigma_e^2 + 1} \\ &= \delta_a^2 - \frac{\delta_a^2 - 1}{1 + \rho_j \sigma_a^2/\sigma_e^2}. \end{aligned} \tag{19}$$

Since δ_a^2 in Equation (19) is greater than one, the maximum ratio $\delta^a_{d_{j*}}$ is achieved with the maximum $\rho_{j_a^*}$ at an optimal level j_a^*. Since $\sigma^2_{d^y_{j,k}} = \sigma_e^2 + \sigma_a^2 \rho_j$ (by Remark 1), the optimal level j_a^* is also the level with the maximum variance of the detail coefficients of the in-control data; i.e., the rule of $j_a^* = \arg\max_j \{\sigma^2_{d^y_{j,k}} | H_0\}$ should be held.

It is worthwhile to notice that Rule 1 provides an optimal selection of the monitoring level of detail coefficients without requiring preknown ARMA models or model estimation. Thus, it is called a model-free approach in this article.

4.1.3. *Select the optimal level of Haar detail coefficients for detecting a variance change of measurement errors*

This subsection presents Rule 2, which explains how the optimal level is selected for monitoring the variance of measurement errors.

Rule 2: The optimal level of Haar detail coefficients for monitoring the variance of measurement errors is selected so that the chosen level has the minimum variance of detail coefficients among all decomposition levels of in-control data; that is,

$$j_e^* = \arg\min_j \left\{ \sigma^2_{d^y_{j,k}} \,\middle|\, H_0 \right\}.$$

Justification: Similar to Rule 1, it is known that the distributions of measurement errors e_t under the in-control condition (H_0) and under a variance change of measurement errors (H_1^2) are

$$\begin{aligned} \mathrm{H}_0 &: e_t \sim N\left(0, \sigma_e^2\right), \\ H_1^2 &: e_t \sim N\left(0, \delta_e^2 \sigma_e^2\right). \end{aligned} \tag{20}$$

It follows Remark 1 that the distributions of the Haar detail coefficient under H_0 and H_1^2 are

$$\begin{aligned} H_0 &: d^y_{j,k} \sim N\left(0, \rho_j \sigma_a^2 + \sigma_e^2\right), \\ H_1^2 &: d^y_{j,k} \sim N\left(0, \rho_j \sigma_a^2 + \delta_e^2 \sigma_e^2\right). \end{aligned} \tag{21}$$

In this case, the variance change ratio $\delta^e_{d_j}$ of the Haar detail coefficients under the H_0 and H_1^2 can be obtained as

$$\begin{aligned} \delta^e_{d_j} &= \frac{\sigma^2_{d^y_{j,k}|H_1^2}}{\sigma^2_{d^y_{j,k}|H_0}} = \frac{\rho_j \sigma_a^2 + \delta_e^2 \sigma_e^2}{\rho_j \sigma_a^2 + \sigma_e^2} = \frac{\delta_e^2 + \rho_j \sigma_a^2/\sigma_e^2}{1 + \rho_j \sigma_a^2/\sigma_e^2} \\ &= 1 + \frac{\delta_e^2 - 1}{1 + \rho_j \sigma_a^2/\sigma_e^2}. \end{aligned} \tag{22}$$

Since δ_e^2 in Equation (22) is greater than one, it can be shown that the maximum ratio $\delta^e_{d_{j*}}$ is achieved with the minimum ρ_{j*} at an optimal level j_e^*. Since $\sigma^2_{d^y_{j,k}} = \sigma_e^2 + \sigma_a^2 \rho_j$ (by Remark 1), the optimal level j_e^* is such a level that has the minimum variance of the detail coefficients of in-control data; i.e., the rule of $j_e^* = \arg\min_j \{\sigma^2_{d^y_{j,k}} | H_0\}$ should be held.

It should be clarified that the maximum $\rho_{j_a^*}$ corresponds to the maximum energy level of Haar detail coefficients close to the characteristic frequency of the normal system response. Therefore, the maximum $\rho_{j_a^*}$ used for Fault 1 detection is generally found after a few steps of Haar wavelet decomposition. It is noted, however, that ρ_j can monotonically decrease after a certain number of decomposition steps and can asymptotically converge to a constant after the frequency band of the detail coefficients is below all

characteristic frequency components. In another aspect, with the increase of the decomposition level, the detection delay of detail coefficients in the time domain also increases. In order to balance these two aspects, an optimal level that is able to detect the change in the variance of measurement errors (Fault 2) and that also has a minimum delay of detection time should be used.

4.2. *Select the optimal level of Haar scale coefficients for mean shift detection*

As discussed in Section 3, the scale coefficients will be used to monitor a process mean shift. The selection of the optimal decomposition level of scale coefficients will be determined by the inherent process characteristic frequency range. In general, the increase of the decomposition level can suppress more autocorrelated noises; however, it also causes a longer detection delay in the time domain. Therefore, an optimal level of Haar scale coefficients is selected with the minimum decomposition level at which the upper boundary of the low-pass filter of the scale coefficients is equal to or less than the lower boundary of the significant frequency responses.

As shown in Fig. 6, if the filter cutoff magnitude is selected as 50% for the Haar transform, the normalized frequency range of the scale coefficients via a low-pass filter is about $[0,\ 1/2^{L+1}]$ at the decomposition level L ($L = 0$ represents the original normalized signal frequency range of [0. 0.5]), whereas the normalized frequency range of detail coefficients via a high-pass filter at each level is $[1/2^{L+1},\ 1/2^{L}]$ ($L \geq 1$). For the mean shift monitoring, it is desirable to choose scale coefficients that have no overlap with the significant characteristic frequency response region; that is, $1/2^{L+1} < \eta_c = f_c/f_{\text{sampling}}$, or $L \geq -\log_2 \eta_c - 1$. Although a higher decomposition level will ensure that the frequency range at that level will be far from the characteristic frequency region, it will also result in a longer detection delay, which is not desirable. Therefore, it is suggested that the decomposition will stop at the lowest level that does not overlap with the characteristic frequency region. In the article, the process is represented by ARMA(2, 1) with $\eta_c = f_c f_c/f_{\text{sampling}} > 0.05$, and thus $L = 4$ can surely satisfy the condition of $1/2^{L+1} < \eta_c$. Therefore, the optimal level j_m^* is selected by $j_m^* = \min[(-\log_2 \eta_c - 1),\ 4]$.

To demonstrate the effectiveness of using scale coefficients to detect a mean shift, 50 in-control observations are randomly generated based on Model 1 with $a_t \sim N(0, 1)$ and $e_t = 0$, followed by the out-of-control data with a mean shift of $\delta_\mu = 1$ from $\tau = 51$. The original data as well as the corresponding Haar scale coefficients obtained at different decomposition levels are shown in Fig. 8. As can be seen from Fig. 8, the process mean shift of $\delta_\mu = 1$ is hardly seen from the original data. This change, however, is more pronounced in the scale coefficients plots. With the increase of the decomposition level of scale coefficients, the mean shift trend is made more obvious by the removal of the high-frequency oscillation pattern.

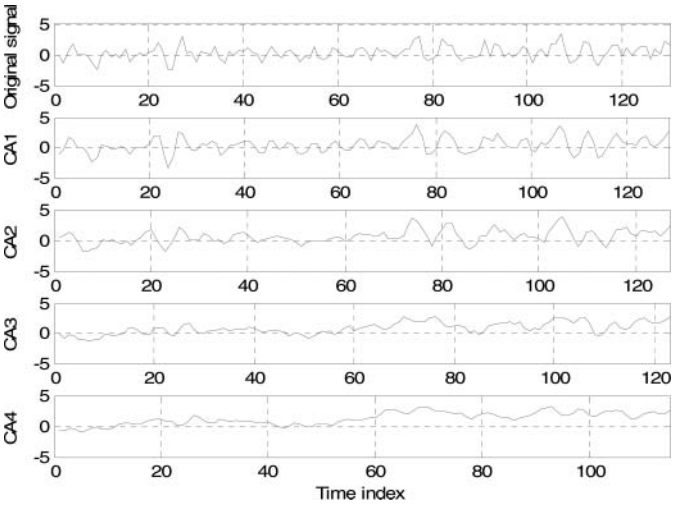

Fig. 8. Haar wavelets decomposition of the signal of Model 1 under the mean shift.

4.3. *Determine the control limits*

The control limit of each chart can be determined such that a specific ARL_0 is obtained. The ARL_0 of each control chart can be approximately set as the inverse of its Type I error rate. In order to achieve a specific Type I error rate for each chart, the overall Type I error rate should be split among control charts, considering the dependency of the monitoring statistics. Since the sample mean is independent of the sample standard deviation, the monitoring statistic for WEWMA is independent of those of SD-WCUSUMs. Therefore, the overall Type I error rate α is obtained by $\alpha = 1 - (1 - \alpha_{\text{WEWMA}})(1 - \alpha_{\text{SD-WCUSUM}})$, where α_{WEWMA} is the Type I error rate of the WEWMA control chart, and $\alpha_{\text{SD-WCUSUM}}$ is the overall Type I error rate corresponding to two SD-WCUSUM control charts used for monitoring the process variance and the variance of measurement errors. The monitoring statistics of the process variance and the variance of measurement errors, however, may be dependent. Thus, based on the Bonferroni inequality, the condition of $\alpha_{\text{SD-WCUSUM}} < (\alpha_{\text{SDp-WCUSUM}}/2) + (\alpha_{\text{SDe-WCUSUM}}/2)$ is used, where $\alpha_{\text{SDp-WCUSUM}}$ and $\alpha_{\text{SDe-WCUSUM}}$ represent the Type I error rate of control charts used for monitoring the variances of process and measurement errors, respectively.

In summary, in order to approximately achieve the given overall Type I error rate α, the Type I error rate corresponding to each control chart should be set as $\alpha_{\text{WEWMA}} = 1 - \sqrt[3]{1-\alpha}$, $\alpha_{\text{SDp-WCUSUM}} = \alpha_{\text{SDe-WCUSUM}} = (1 - \sqrt[3]{(1-\alpha)^2})/2$. With these choices of the Type I error rate for each control chart, the overall ARL_0 corresponding to these three charts is approximated by $1/\alpha$. It should be noted that this is an approximate equation since the

monitoring statistics in both WEWMA and SD-WCUSUM control charts are autocorrelated over the sampling time.

5. Simulation study

The following case studies will be used to illustrate the effectiveness of the proposed methods for detecting a change in the process variance, variance of measurement errors, and process mean, respectively. The comparison with other existing control charts will also be given. The models in Table 1 were used in the following simulations. In this section, the reference value K in all CUSUM charts was set to 0.5 and the value of λ in all EWMA charts was set to 0.20. As we compare the proposed control charts with existing control charts one by one, without loss of generality, the ARL_0 of each control chart was set to be approximately equal to 370. We used Monte Carlo simulations to obtain the control limits since the monitoring statistics in all control charts are autocorrelated. In all of the following three cases, it was assumed that, when the process is under the in-control condition (H_0), a_t follow the distribution of $N(0, 1)$ and measurement errors e_t follow the distribution of $N(0, 0.5^2)$.

Case 1: Optimal level selection for detecting a process variance change.

As discussed before (Remark 1 and Rule 1), the detection power for monitoring a process variance change is different at different decomposition levels. Model 1 was chosen to illustrate how to select an optimal level for detecting a change in the process variance. Assume under the fault condition (H_1^1) that a_t changes from $N(0, 1)$ to $N(0, 1.5^2)$ with $\delta_a = 1.5$ from time $\tau = 51$. Based on the simulated in-control data (H_0), the variance of Haar detail coefficients for the first four detail levels were obtained, which are 1.15, 2.21, 2.38, and 1.22, respectively. Based on Rule 1, the optimal level with the maximum detail coefficient variance should be selected, which in this case is Level 3.

To compare the detection performance of the optimal level with that of other levels, we constructed four SD-CUSUM charts for each level of detail coefficients, as shown in Fig. 9(a). The control limits of h values were 5.07, 7.30, 9.79, and 10.39 at each level, respectively. From Fig. 9(a), it can be seen that although the process variance change can be detected at both Level 2 and Level 3, Level 3 (CD3) shows the largest change among all levels of detail coefficients. Based on Rule 1, it is suggested that the SD-CUSUM chart be applied at the optimal Level 3 rather than at all levels. Similar results were obtained when Model 2 was used; the variances of the detail coefficients for the first four levels were obtained as 4.37, 7.39, 0.74, and 0.71, respectively. As shown in Fig. 9(b), Level 2, which has the maximum variance of detail coefficients of in-control data, has the best detection ability.

Case 2: Optimal level selection for detecting a variance change in measurement errors.

In this case, Model 1 was initially investigated under the fault condition (H_1^2), with e_t being changed from $N(0, 0.5^2)$ to $N(0, 1.5^2)$ at time $\tau = 51$. From Case 1, it was known that the variances of Haar detail coefficients under H_0 at the first four levels are 1.15, 2.21, 2.38, and 1.22, respectively. Based on Rule 2, the level with the minimum variance of detail coefficients should be selected, which is Level 1. For comparison, we constructed four SD-CUSUM charts for each level of detail coefficients. From Fig. 10(a), it can be seen that the control chart based on the detail coefficients at Level 1 has the largest change. A similar analysis was conducted for Model 2. The selected optimal level of Model 2 is Level 4 because the variance of detail coefficients at

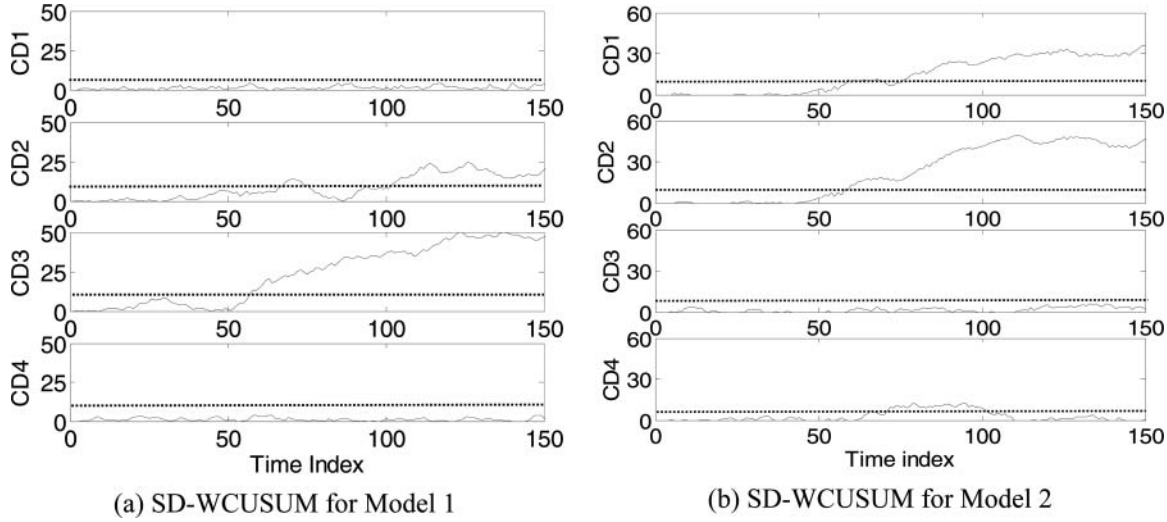

(a) SD-WCUSUM for Model 1 (b) SD-WCUSUM for Model 2

Fig. 9. Comparison of different levels of Haar detail coefficients in detecting a process variance change (Fault 1).

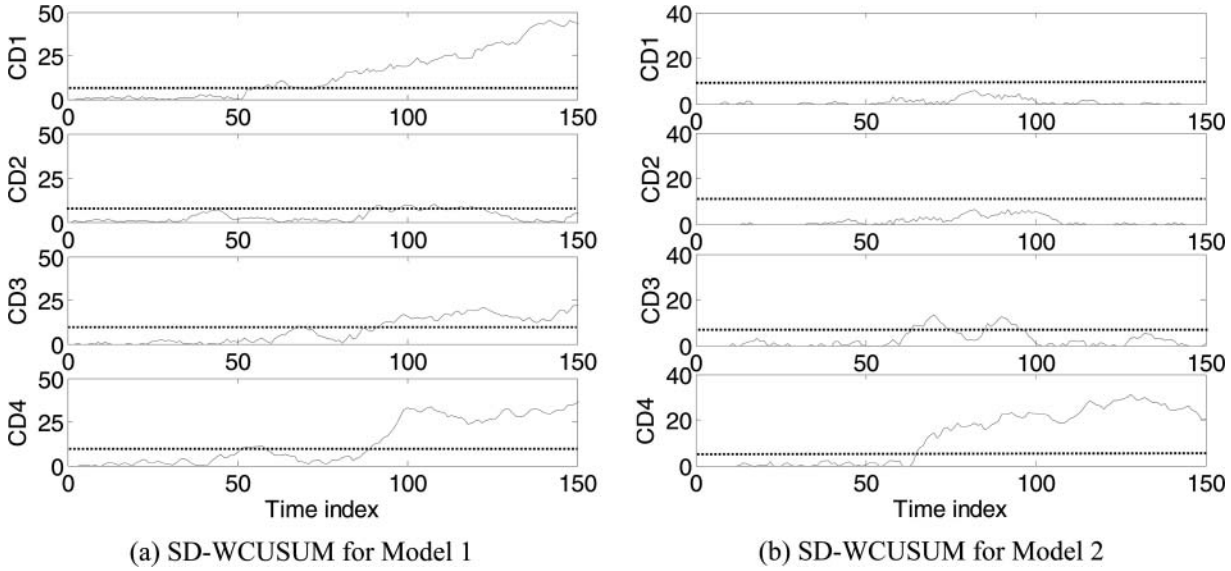

Fig. 10. Comparison of different levels of Haar detail coefficients in detecting a variance change of measurement errors (Fault 2).

Level 4 is the minimum among all four levels (4.37, 7.39, 0.74, and 0.71). As shown in Fig. 10(b), Level 4 with the minimum variance of detail coefficients of in-control data has the most obvious trend in the SD-WCUSUM chart.

Case 3: Comparison between SD-MCUSUM and SD-CUSUM for process variance monitoring.

This case serves primarily to show that the proposed variance monitoring chart of SD-WCUSUM is robust when applied to a process with a mean shift. It was assumed that the process noise a_t had a mean shift from time $\tau = 51$ following the distribution of $a_t \sim N(1.5, 1)$ ($\delta_\mu = 1.5$) without any variance change. The control limits (h) of SD-CUSUM and SD-WCUSUM for monitoring the process variance were set to 7.30 and 7.02, respectively, when Model 1 was used. Figures 11(a) and 11(b) plot the SD-WCUSUM and SD-WCUSUM charts based on the selected detail coefficients, in which the detail coefficients at Level 3 were used for Model 1. It can be seen that the traditional SD-CUSUM chart is sensitive to the process mean shift (Fig. 11(b)), although there is no process variance change. That is, it generates a false alarm for process variance change. In contrast, the proposed SD-WCUSUM chart does not show an out-of-control signal; i.e., SD-WCUSUM is only sensitive to the process variance change but is robust to the process mean shift. Therefore, SD-WCUSUM has a good diagnostic capability to separate between a process variance change and a mean shift.

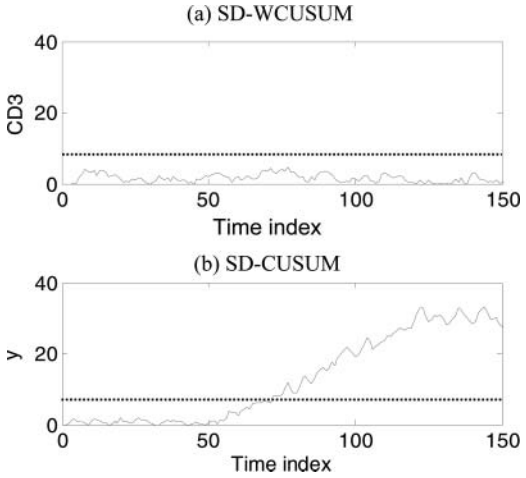

Fig. 11. Robustness comparison of SD-WCUSUM and SD-CUSUM to mean shift.

A further study was carried out to compare the robustness of SD-WCUSUM and SD-CUSUM in terms of their ARLs. In this study, the simulation data were generated based on both Model 1 and Model 2 when the process has a mean shift with different magnitudes of δ_μ but without any change on the process variance. Therefore, it would be expected that the variance monitoring charts should ideally be in an in-control state in most of the samples; i.e., the ARL value should be close to the designed ARL_0 ($ARL_0 = 370$ is used in this article) even though the process mean has a mean shift δ_μ. Figure 12 shows the ARL_0 values for process variance monitoring when the process variance is under the in-control condition and its robustness performance under the different values of δ_μ. The solid and dashed lines in Fig. 12 represent the ARL values of the SD-CUSUM and SD-WCUSUM control charts, respectively. The standard error of ARL_0 estimates in each case is less than 1% of ARL_0 based on 10 000 simulation replications. As can be seen from Fig. 12, the ARL values of SD-WCUSUM are kept around 370 under different mean

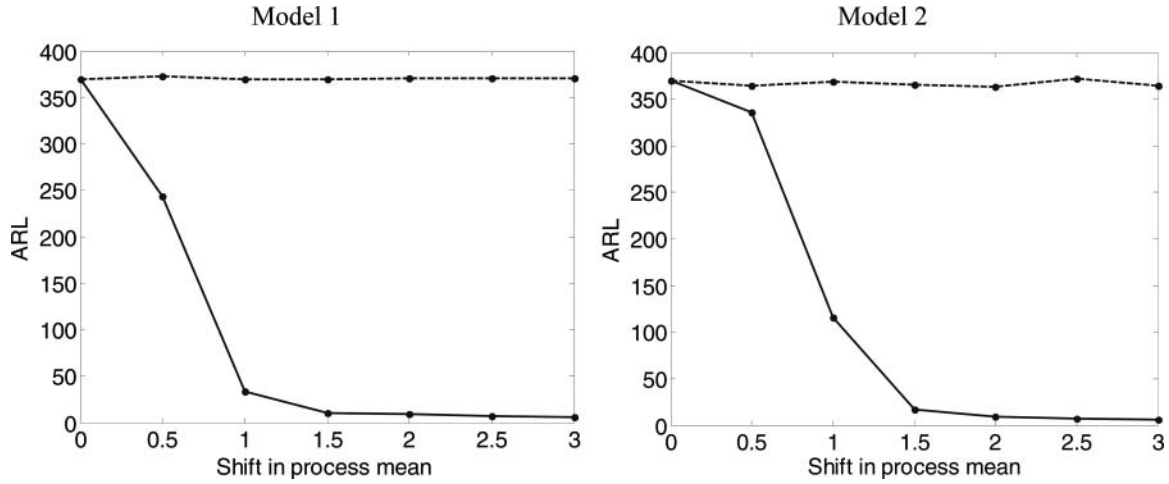

Fig. 12. Performance comparison in terms of the robustness to a mean shift between SD-CUSUM (solid line) and SD-WCUSUM (dashed line) in detecting a process variance change.

shifts, whereas the ARL values of SD-CUSUM quickly decrease with the increase of mean shifts. This implies that SD-CUSUM, though designed for variance monitoring, is not robust to mean shifts. In other words, if an alarm signal is received from SD-CUSUM, it is not clear whether this alarm signal is genuinely because of a change in the process variance or in the process mean. Therefore, SD-CUSUM cannot be used for diagnosis. In contrast, a process mean shift does not affect the performance of SD-WCUSUM for monitoring the process variance. Therefore, an alarm signal from the SD-WCUSUM chart can be directly interpreted as a possible change in the process variance.

We also compared the performance of SD-CUSUM and SD-WCUSM in detecting a process variance change when the process mean is in an in-control state, as shown in Fig. 13. By combining the results of Fig. 12 and Fig. 13, it can be seen that both SD-WCUSUM and SD-CUSUM charts have a similar ARL performance for detecting a process variance change; the SD-WCUSUM chart, however, shows a better performance than the SD-CUSUM chart in terms of their robustness to a process mean shift.

Case 4: Comparison of SD-CUSUM and SD-WCUSUM in monitoring the variance of measurement errors.

In this subsection, the performances of SD-CUSUM and SD-WCUSUM control charts in detecting a variance change of measurement errors are studied. Assume that the process is changed into an out-of-control condition of (H_1^2) with $e_t \sim N(0, \delta_e^2 0.5^2)$. Models 1 and 2 were used for this simulation study and each simulation was repeated 10 000 times. The standard error of ARL estimates in each case is less than 1% of ARL. The out-of-control ARL plots for different change magnitudes of δ_e are depicted in Fig. 14. It is clear from the figure that SD-WCUSUM outperforms SD-CUSUM in detecting the variance change in measurement errors. This superiority is more pronounced when Model 2

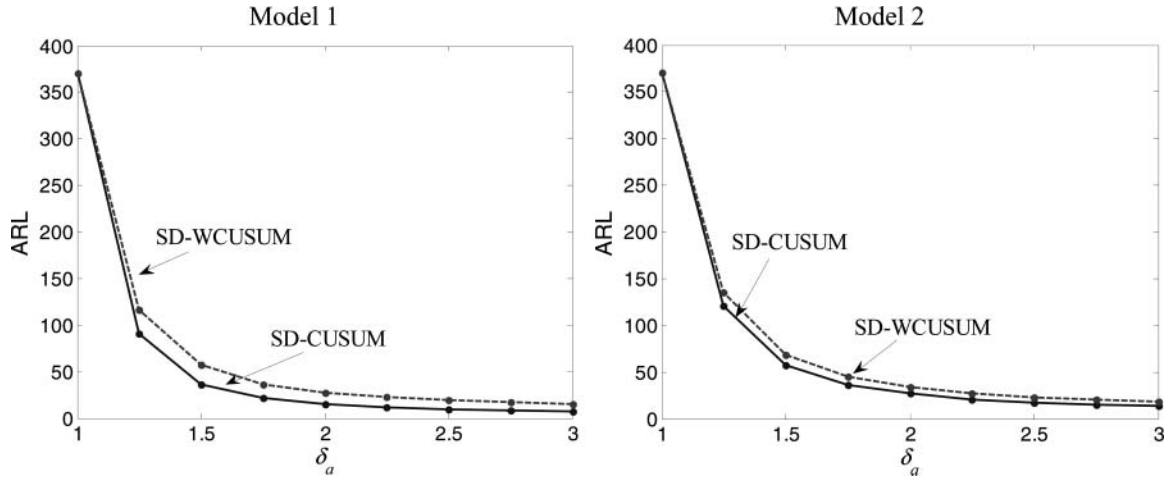

Fig. 13. Similar detection performance for both SD-CUSUM and SD-WCUSUM in detecting a process variance change.

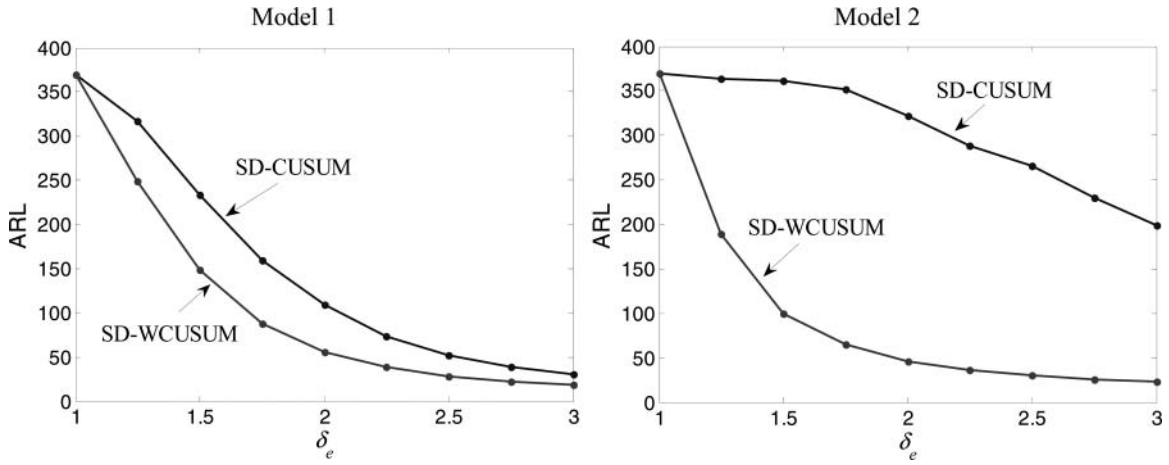

Fig. 14. Better detection performance of SD-WCUSUM than SD-CUSUM in detecting a variance change of measurement errors.

is used since the variance ratio of detail coefficients at the optimal level $d^y_{j*,k}$ to the total variance in Model 2 is less than that of Model 1.

Case 5: Comparison of WEWMA with Direct-EWMA and SCC-EWMA charts.

In order to quantitatively demonstrate the effectiveness of the mean shift detection using scale coefficients, the out-of-control ARL performance of the WEWMA chart is compared with that of Direct-EWMA charts. Moreover, the out-of-control ARL performance of the SCC-EWMA chart using the true process model structure and the estimated model parameters used to whiten the autocorrelated data is also compared. For all three methods, 10 000 runs were used to obtain the average and standard deviation of the run length. The standard error of ARL estimates in each case is less than 1% of ARL. As shown in Fig. 15, it is clear that WEWMA always shows a better ARL performance than the Direct-EWMA chart. WEWMA achieves comparable performance to that of the SCC-EWMA, although with a slightly longer detection delay. However, prior knowledge of the process model is required for SCC-EWMA, which is not available in many practical cases.

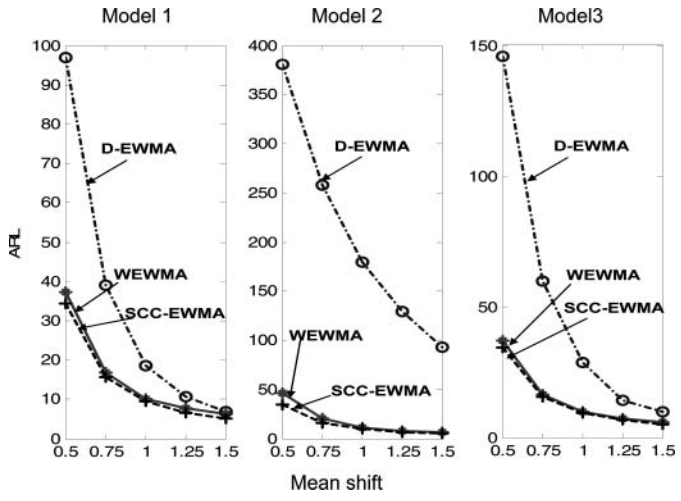

Fig. 15. ARL comparison of WEWMA, direct EWMA, and SCC EWMA.

6. Conclusions

In this article, a multiscale SPC monitoring method using Haar wavelets analysis has been developed to detect both process mean shifts and variance changes. Three monitoring charts are developed to separately detect changes in the process mean, the process variance, and the variance of measurement errors, simultaneously. Based on the different frequency characteristics of scale coefficients and detail coefficients, one WEWMA chart is developed to monitor the selected scale coefficients for detecting a process mean shift, and two SD-WCUSUM charts are developed to monitor the optimally selected levels of detail coefficients for detecting a variance change. The optimal selection of the monitoring levels requires neither a model structure nor model estimation. Our simulation results indicate the superiority of the proposed SD-WCUSUM chart over the traditional SD-CUSUM chart in the following two aspects: (i) its robustness to process mean shifts in monitoring process variance; and (ii) its better detection power in monitoring the variance of measurement errors. Therefore, SD-WCUSUM has a better diagnosis capability for identifying the process change between a mean shift, a variance change, or both changes. Moreover, for comparing the performance of control charts in monitoring the process mean, our simulation results show that the proposed WEWMA chart is more powerful in detecting a small mean shift by monitoring the selected scale coefficients than the traditional EWMA chart that directly monitors original signals.

It should also be pointed out that the main contribution of this research is to develop a model-free approach by selecting effective monitoring features from Haar wavelet coefficients rather than simply using the original signals, or whitened residuals, or all levels of Haar wavelet coefficients. Although time series modeling is used as the theoretical basis for our analysis and mathematical derivation, in practical implementation, the selection of optimal monitoring level does not need a preknown process model or additional time series modeling effort. In future work, a general multiscale control chart system will be further investigated for any ARMA(n, m) model with $n > 2$.

Acknowledgements

The authors would like to gratefully acknowledge the financial support of NSF PECASE/CAREER AWARD DMI 0549306, NSF DMI F0541750, and Michigan 21st Century Jobs Fund F015886. The authors would also like to thank the department editor and referees for their insightful comments.

References

Adams, B.M. and Tseng, L.T. (1998) Robustness of forecast-based monitoring schemes. *Journal of Quality Technology*, **30**, 328–339.

Alwan, L.C. and Roberts, H.V. (1988) Time series modeling for statistical process control. *Journal of Business and Economics Statistics*, **6**, 87–95.

Apley, D.W. and Shi, J. (1999) The GLRT for statistical process control of autocorrelated processes. *IIE Transactions*, **31**, 1123–1134.

Bakshi, B.R. (1998) Multiscale PCA with application to multivariate statistical process monitoring. *AIChE Journal*, **44**(7), 1596–1610.

Bakshi, B.R. (1999) Multiscale analysis and modeling using wavelets. *Journal of Chemometrics*, **13**, 414–434.

Box, G., Jenkins, G. and Reinsel, G. (1994) *Time Series Analysis, Forecasting, and Control*, third edition, Prentice-Hall, Englewood Cliffs, NJ.

Capizzi, G. and Masarotto, G. (2003) An adaptive exponentially weighted moving average control chart. *Technometrics*, **45**, 199–207.

Chicken, E., Pignatiello, J.J. and Simpson, J.R. (2009) Statistical process monitoring of nonlinear profiles using wavelets. *Journal of Quality Technology*, **41**, 198–212.

Daubechies, I. (1992) *Ten Lectures on Wavelets*, Society for Industrial and Applied Mathematics, Philadelphia.

Dyer, J.N., Adams, B.M. and Conerly, M.D. (2003) The reverse moving average control chart for monitoring autocorrelated processes. *Journal of Quality Technology*, **35**, 139–152.

Ganesan, R., Das, T.K., Sikder, A.K. and Kumar, A. (2003) Wavelet-based identification of delamination defect in CMP (Cu-Low k) using nonstationary acoustic emission signal. *IEEE Transactions on Semiconductor Manufacturing*, **16**, 41–57.

Hawkins, D.M. (1981) A CUSUM for a scale parameter. *Journal of Quality Control*, **13**, 228–231.

Hawkins, D.M. (1993) Cumulative sum control charting: an underutilized SPC tool. *Quality Engineering*, **5**, 463–467.

Hawkins, D.M. and Zamba, K.D. (2005) Statistical process control for shifts in mean or variance using a changepoint formulation. *Technometrics*, **47**, 164–172.

Hwarng, B. (2005) Simultaneous identification of mean shift and correlation change in AR(1) processes. *International Journal of Production Research*, **43**, 1761–1783.

Jeong, M.K., Lu, J.C., and Wang, N. (2006) Wavelet-based SPC procedure for complicated functional data. *International Journal of Production Research*, **44**, 729–744.

Jin, J. and Shi, J. (2001) Automatic feature extraction of waveform signals for in-process diagnostic performance improvement. *Journal of Intelligent Manufacturing*, **12**, 257–268.

Lada, E.K., Lu, J.C. and Wilson, J.R. (2002) A wavelet-based procedure for process fault detection. *IEEE Transactions on Semiconductor Manufacturing*, **15**, 79–90.

Lu, C.W. and Reynolds, M.R. (1999) Control charts for monitoring the mean and variance of autocorrelated processes. *Journal of Quality Technology*, **31**, 259–274.

Luo, R.F., Misra, M. and Himmelblau, D. (1999) Sensor fault detection via multiscale analysis and dynamic PCA. *Industrial Engineering of Chemical Research*, **38**, 1489–1496.

Montgomery, D.C. (2005) *Introduction to Statistical Quality Control*, fifth edition, John Wiley & Sons, New York, NY.

Pandit, S.M. and Wu, S.M. (1983) *Time Series and System Analysis with Applications*, John Wiley & Sons, New York, NY.

Reynolds, M.R. and Stoumbos, Z.G. (2006) Comparisons of some exponentially weighted moving average control charts for monitoring the process mean and variance. *Technometrics*, **48**, 550–567.

Runger, G.C. and Willemain, T.R. (1996) Batch-means control charts for autocorrelated data. *IIE Transactions*, **28**, 483–487.

Schmid, W. (1997) On EWMA charts for times series, in *Frontiers in Statistical Quality Control*, Vol. 5, Lenz, H.J. and Wilrich, P.T. (eds), Physica-Verlag, Heidelberg, Germany, pp. 115–137.

Wardell, D.G., Moskowitz, H. and Plante, R.D. (1992) Control charts in the presence of Data correlation. *Management Science*, **38**, 1084–1105.

Zhang, N.F. (1998) A statistical control chart for stationary process data. *Technometrics*, **40**, 24–38.

Biographies

Dr. Huairui (Harry) Guo is the Director of the Theoretical Development Department at ReliaSoft Corporation. He received his Ph.D. in Systems & Industrial Engineering and M.S. in Reliability & Quality Engineering, both from the University of Arizona. His research and publications cover reliability areas, such as life data analysis, repairable system modeling, and reliability test planning, and quality areas, such as process monitoring, analysis of variance and design of experiments. In addition to research and product development, he is also part of the training and consulting arm and has been involved in various projects from automobile, medical devices, oil and gas, and aerospace industries. He is a certified reliability professional.

Kamran (Kami) Paynabar is a Ph.D. candidate in the Department of Industrial and Operations Engineering at the University of Michigan. He received his B.Sc. and M.Sc. in Industrial Engineering at Iran University of Science and Technology and Azad University in 2002 and 2004, respectively, and his M.A. in Statistics at the University of Michigan in 2010. His research interests include developing new approaches for system modeling, process monitoring, and fault diagnosis of manufacturing and health-care systems. His research expertise is in the area of variation modeling and fault diagnosis of high-dimensional functional data and waveform signals by integrating statistical learning techniques and enigneering models. He is a member of ASQ, IIE, and INFORMS.

Jionghua (Judy) Jin is a Professor in the Department of Industrial and Operations Engineering at the University of Michigan. She received her Ph.D. degree from the University of Michigan in 1999. Her recent research focuses on data fusion for improving complex system operations, which includes variation reduction, condition monitoring and fault diagnosis, process control, knowledge discovery, and decision making. Her research emphasizes a multidisciplinary approach by integrating applied statistics, signal processing, reliability engineering, system control, and decision-making theory. She has received a number of awards including the NSF CAREER Award in 2002 and the PECASE Award in 2004 and seven Best Paper Awards during 2005–2010. She is a member of ASME, ASQ, IEEE, IIE, INFORMS, and SME.